

Wigner Function Analysis of Finite Matter-Radiation Systems

E. Nahmad-Achar^{1*}, R. López-Peña¹, S. Cordero¹, and O. Castaños¹

1 Instituto de Ciencias Nucleares
 Universidad Nacional Autónoma de México
 Apartado Postal 70-543, México 04510 CDMX
 * nahmad@nucleares.unam.mx

February 9, 2023

1



34th International Colloquium on Group Theoretical Methods in Physics
 Strasbourg, 18-22 July 2022
 doi:10.21468/SciPostPhysProc.?

2

3 Abstract

4 We show that the behaviour in phase space of the Wigner function associated to the
 5 electromagnetic modes carries the information of both, the entanglement properties be-
 6 tween matter and field, and the regions in parameter space where quantum phase tran-
 7 sitions take place. A finer classification for the continuous phase transitions is obtained
 8 through the computation of the surface of minimum fidelity.

9

10 Contents

11	1 Introduction	1
12	2 The Generalised Dicke Model	2
13	2.1 Variational Study	3
14	2.2 Numerical Quantum Solution	3
15	3 Fidelity as Signature of QPT in Finite Systems	4
16	4 Wigner Function in the Λ-Configuration	5
17	4.1 Correlation between Wigner Function and Entanglement	6
18	5 Conclusion	8
19	References	8

20

21

22 1 Introduction

23 Quantum phase transitions (QPT) are studied in nuclear, molecular, quantum optics, and con-
 24 densed matter physics, and have potential applications in the design of quantum technolo-
 25 gies [1]. The Wigner function gives a complete description of a quantum system in phase

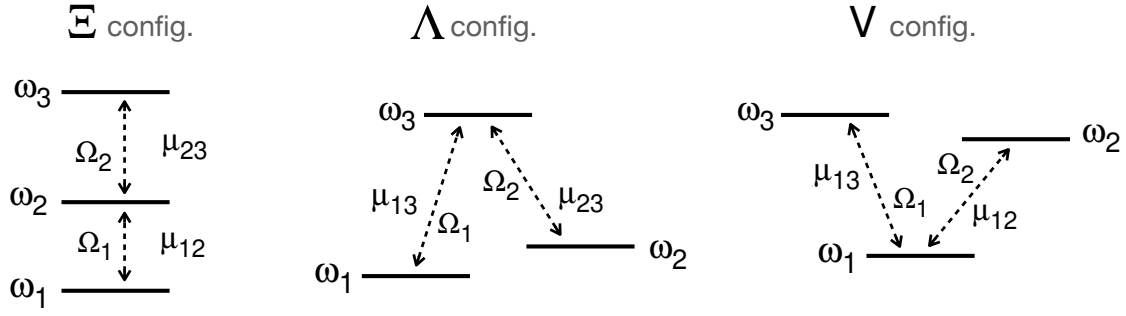


Figure 1: Atomic configurations for 3-level systems, showing the possible transitions and coupling strengths μ_{ij} .

26 space; it allows for the calculation of all the quantities that the usual wave function gives,
 27 and negative values in the function appear as a consequence of interference between distant
 28 points in phase space. In a generalized Dicke model of 3-level atoms interacting with 2 electro-
 29 magnetic modes, it may be used to analyse the behaviour in phase space of the two radiation
 30 modes of light across the finite phase diagram of the quantum ground state, and supply further
 31 evidence of the quantum phase transitions revealed by the fidelity criterion.

32 When the linear entropy for all the subsystems is calculated and compared with the beh-
 33aviour of the Wigner function, we see that the entanglement between the substates responds
 34 to how the bulk of the ground state changes from a subset of the basis with a major contribution
 35 from one kind of photons, to a subset with a major contribution of the other one.

36 2 The Generalised Dicke Model

The multipolar Hamiltonian for the dipole interaction between a 2-mode radiation field and a
 3-level atomic system in the long wave approximation ($\hbar = 1$) is

$$\mathbf{H} = \mathbf{H}_D + \mathbf{H}_{int}$$

with

$$\mathbf{H}_D = \sum_{j < k}^3 \Omega_{jk} \mathbf{a}_{jk}^\dagger \mathbf{a}_{jk} + \sum_{j=1}^3 \omega_j \mathbf{A}_{jj}$$

and

$$\mathbf{H}_{int} = -\frac{1}{\sqrt{N_a}} \sum_{j < k}^3 \mu_{jk} (\mathbf{A}_{jk} + \mathbf{A}_{kj}) (\mathbf{a}_{jk} + \mathbf{a}_{jk}^\dagger)$$

37 Here, N_a denotes the number of particles, \mathbf{a}_{jk}^\dagger , \mathbf{a}_{jk} are creation and annihilation photon oper-
 38 ators, Ω_{jk} is the frequency of the mode which promotes transitions between the atomic levels
 39 ω_j and ω_k , \mathbf{A}_{ij} are the matter operators obeying the $U(3)$ algebra, with $\sum_{k=1}^3 \mathbf{A}_{kk} = N_a \mathbf{I}_{matter}$,
 40 and μ_{ij} is the coupling parameter between atomic levels ω_j and ω_k .

41 We have the atomic configurations shown in Figure 1, customarily labelled by Ξ , Λ , and
 42 V , due to their shape resembling these letters, and where we label the atomic energy levels
 43 following $\omega_1 \leq \omega_2 \leq \omega_3$ and for simplicity fix $\omega_1 = 0$ and $\omega_3 = 1$; therefore, all energies are
 44 measured in terms of $\hbar\omega_3$. Note that particular atomic configurations are obtained by making
 45 an appropriate dipolar strength μ_{ij} vanish.

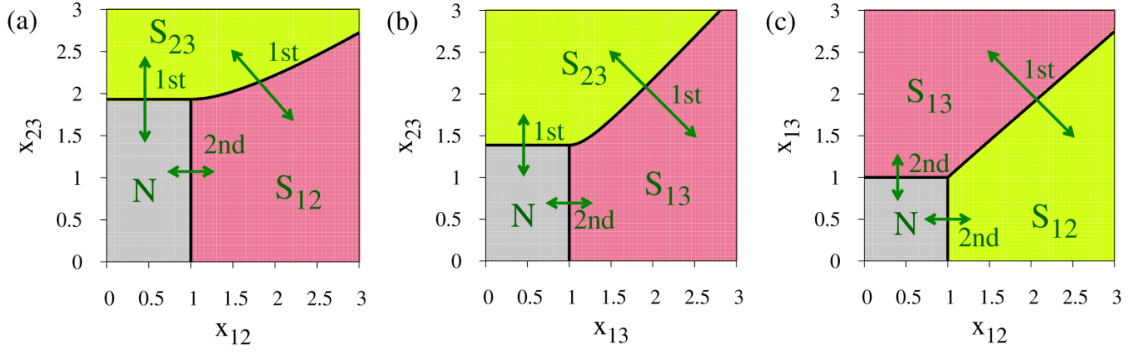


Figure 2: Phase diagrams from a variational study using coherent test states, for the different atomic configurations Ξ , Λ , and V (from left to right). The order of the transitions according to the Ehrenfest classification is shown. The parameters used are: Ξ -configuration: $\omega_2/\omega_3 = 1/3$; Λ -configuration: $\omega_2/\omega_3 = 1/10$; V -configuration: $\omega_2/\omega_3 = 8/10$. Here, $x_{ij} = \mu_{ij}/\mu_c$ is the dimensionless dipolar coupling strength, where μ_c stands for its critical value in the two-level system $\{ij\}$ in the limit $N_a \rightarrow \infty$.

46 2.1 Variational Study

47 A variational study involving coherent states for both matter and field provides a good ap-
 48 proximation of the ground state energy surface per particle [2, 3]. Figure 2 shows the phase
 49 diagrams from a variational study using coherent test states, for the different atomic configu-
 50 rations Ξ , Λ , and V (from left to right), as well as the order of the transitions according to the
 51 Ehrenfest classification. We distinguish a *normal* region (N , in medium grey) where the atoms
 52 decay individually, and *collective* regions S_{ij} where the decay is proportional to $N_a(N_a + 1)$
 53 and in which only one kind of photon contributes to the ground state. Continuous black lines
 54 denote the separatrices dividing these regions.

55 It is important to note that the signature of the phase diagram remains when the symme-
 56 tries of the Hamiltonian are restored in the variational solution and the thermodynamic limit
 57 $N_a \rightarrow \infty$ is taken.

58 2.2 Numerical Quantum Solution

59 The exact calculation of the ground state involves a numerical diagonalisation of the Hamil-
 60 tonian matrix. The Hamiltonian is invariant under parity transformations of the form

$$\Pi_1 = e^{i\pi\mathbf{K}_1}, \quad \Pi_2 = e^{i\pi\mathbf{K}_2}$$

61 where \mathbf{K}_s , $s = 1, 2$, are constants of motion when the rotating wave approximation (RWA) is
 62 taken. Accordingly, the Hilbert space \mathcal{H} divides naturally into four subspaces

$$\mathcal{H} = \mathcal{H}_{ee} \oplus \mathcal{H}_{eo} \oplus \mathcal{H}_{oe} \oplus \mathcal{H}_{oo},$$

63 where subscripts $\sigma = \{ee, eo, oe, oo\}$ denote the even e or odd o parity of Π_1 and Π_2 , respec-
 64 tively.

65 We use basis states labeled by $|\nu_{12}, \nu_{13}, \nu_{23}\rangle \otimes |n_1, n_2, n_3\rangle$, with $n_1 + n_2 + n_3 = N_a$ and
 66 $\nu_{jk} = 0, 1, \dots, \infty$, which denote Fock states.

67 Since the dimension of the Hilbert space is $\dim(\mathcal{H}) = \infty$, we need to use a truncation
 68 criterion. For the set of eigenvalues of \mathbf{K}_1 , \mathbf{K}_2 , we take this criterion as follows: choose values
 69 $k_{i\max}$ to satisfy

$$1 - \mathcal{F}(k_{1\max}, k_{2\max}) \leq 10^{-10},$$

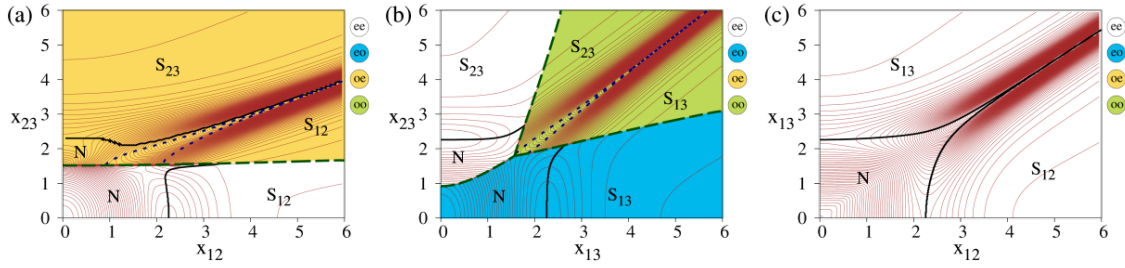


Figure 3: Quantum phase diagrams for the three atomic configurations, Ξ , Λ , and V (from left to right), for one atom when in resonance with the field modes. Different types of transitions are shown (see text). For the Ξ -configuration we have used $\Omega_{12} = 1/4$, $\Omega_{23} = 3/4$ and $\omega_2 = 1/4$; for the Λ -configuration $\Omega_{13} = 1$, $\Omega_{23} = 9/10$, and $\omega_2 = 1/10$; and for the V -configuration $\Omega_{12} = 4/5$, $\Omega_{13} = 1$ and $\omega_2 = 4/5$.

70 where $\mathcal{F}(k_1, k_2) = |\langle \psi(k_1, k_2) | \psi(k_1 + 2, k_2 + 2) \rangle|^2$ is the fidelity between the state $|\psi(k_1, k_2)\rangle$
 71 containing all eigenvalues up to k_1 and k_2 , and the state $|\psi(k_1 + 2, k_2 + 2)\rangle$. This ensures that
 72 the energy calculated remains without variation to one part in 10^{-8} . Other criteria may be
 73 used, of course, depending on the problem in question.

74 3 Fidelity as Signature of QPT in *Finite* Systems

75 Quantum phase transitions are determined by singularities in the wave function of the ground
 76 state, and these may be studied by the method of Ginzburg-Landau, or using catastrophe
 77 theory, in the thermodynamic limit [4]. Another criterion is by the loci where the fidelity
 78 between neighbouring states $|\Psi_g(\xi_1)\rangle, |\Psi_g(\xi_2)\rangle$ along parametric lines $\xi(t)$ in parameter space

$$\mathcal{F}(\rho_{\xi(t)}, \rho_{\xi(t+\delta)}) = |\langle \Psi_g(\xi(t)) | \Psi_g(\xi(t + \delta)) \rangle|^2$$

79 presents a minimum (see e.g. [5, 6] and references therein). We have followed this method
 80 for *finite* systems to find the separatrices in parameter space. We call these *quantum phase*
 81 *transitions*, in contrast to other terminology that appears in the literature, since the consti-
 82 tution of the ground state changes significantly as one crosses a separatrix. The *surface of*
 83 *minimum fidelity* is calculated by considering neighbouring points in directions parallel to the
 84 axes ($x_{jk} = 0$), along identity lines, and along their orthogonal directions, thereby finding the
 85 local minima. Here, $x_{jk} = \mu_{jk}/\mu_c$, where

$$\mu_c = \frac{1}{2} \sqrt{\Omega_{jk}(\omega_k - \omega_j)}$$

86 stands for the critical coupling value in a two-level $\{jk\}$ system, in the limit $N_a \rightarrow \infty$. Thus,
 87 x_{jk} is the dimensionless dipolar coupling.

88 In the case of the generalised *quantum* Rabi model, the quantum separatrices for a single 3-
 89 level atom interacting dipolarly with two modes of electromagnetic field are given in Figure 3,
 90 for the three atomic configurations, Ξ , Λ , and V (from left to right), when in resonance with
 91 the field modes [7]. The parity of the Hilbert subspace in which the ground state lives is
 92 marked by colours and by the letters $\{ee, eo, oe, oo\}$, and we see that a much richer structure
 93 appears in contrast with the limit $N_a \rightarrow \infty$ shown in Fig. 2.

94 Quantum phase transitions for a finite system appear where the ground state changes
 95 abruptly, and this may be determined by calculating the fidelity or the fidelity susceptibility
 96 between neighbouring states. We can distinguish three types of loci of points where this takes
 97 place (cf. Figure 3):

- 98 1. Dashed lines: *discontinuous transitions*, the fidelity between neighbouring states falls
 99 to zero, and the separatrix in this case borders along orthogonal Hilbert subspaces of
 100 different parity;
- 101 2. Continuous lines: *stable continuous transitions*, $F(\xi) \neq 0$ and it remains different from
 102 zero as N_a increases;
- 103 3. Dotted lines: *unstable continuous transitions*, $F(\xi) \neq 0$ but reaches zero in the large N_a
 104 limit.

105 This classification is further corroborated through the behaviour of the Wigner function for
 106 each field mode, as we shall see in the next section. Note that stable and unstable continuous
 107 transitions can also be distinguished by means of the Bures distance, which measures the dif-
 108 ference of two probability densities of the quantum system; for the stable continuous transition
 109 the value of the Bures distance will be smaller than for the unstable continuous transition.

110 4 Wigner Function in the Λ -Configuration

111 First order quantum phase transitions, according to the Ehrenfest classification, can be always
 112 associated to zero fidelity values, i.e., discontinuous transitions, and the corresponding eigen-
 113 states are orthogonal.

114 A finer classification of the continuous transitions is more evident through the study of
 115 the *Wigner function*, since this classification is based on whether the bulk of the ground state
 116 remains in a sub-basis of the total basis or not. Here we shall focus on the Λ configuration,
 117 which appears to have a richer structure.

118 We may use the parity operators for the Λ -configuration

$$\begin{aligned} \mathbf{K}_1 &= \nu_{13} + \nu_{23} + \mathbf{A}_{33} , \\ \mathbf{K}_2 &= \nu_{23} + \mathbf{A}_{11} + \mathbf{A}_{33} , \end{aligned}$$

119 to replace the electromagnetic quanta oscillation numbers

$$\nu_{13} = k_1 - k_2 + n_1 , \quad \nu_{23} = k_2 - n_1 - n_3 ,$$

120 and thus denote the ground state of the system as

$$|\psi_{\text{gs}}\rangle = \sum_{k_1, k_2} \sum_{n_1, n_3}^{N_a} C_{k_1, k_2, n_1, n_3} \times |k_1 - k_2 + n_1, k_2 - n_1 - n_3, n_1, N_a - n_1 - n_3, n_3\rangle ,$$

121 from which we calculate the reduced density matrices ϱ_{jk} ($j < k$) for modes ν_{jk} .

122 Notice that for the case of a single atom, for maximum values of $x_{jk} = 6$ and for the desired
 123 precision of 10^{-10} established in Sec. 2.2, the ground state function lives in a Hilbert space
 124 of dimension $\dim(\mathcal{H}) = 1395$, while for a precision of 10^{-15} the dimension must at least be
 125 $\dim(\mathcal{H}) = 2079$ [8].

126 Thus, the Wigner functions for the reduced density matrices are

$$\begin{aligned} W_{13}(q, p) &= \sum_{k_1, k_2, k'_1} \sum_{n_1, n_3} C_{k_1, k_2, n_1, n_3} C_{k'_1, k_2, n_1, n_3}^* W_{|k_1 - k_2 + n_1\rangle \langle k'_1 - k_2 + n_1|}(q, p) , \\ W_{23}(q, p) &= \sum_{k_1, k_2, k'_2} \sum_{n_1, n_3} C_{k_1, k_2, n_1, n_3} C_{k'_2, k_2, n_1, n_3}^* W_{|k_2 - n_1 - n_3\rangle \langle k'_2 - n_1 - n_3|}(q, p) . \end{aligned}$$

127 where $W_{|n\rangle \langle m|}(q, p)$ is the Weyl symbol for the operator $\rho_{nm} = |n\rangle \langle m|$ [9, 10].

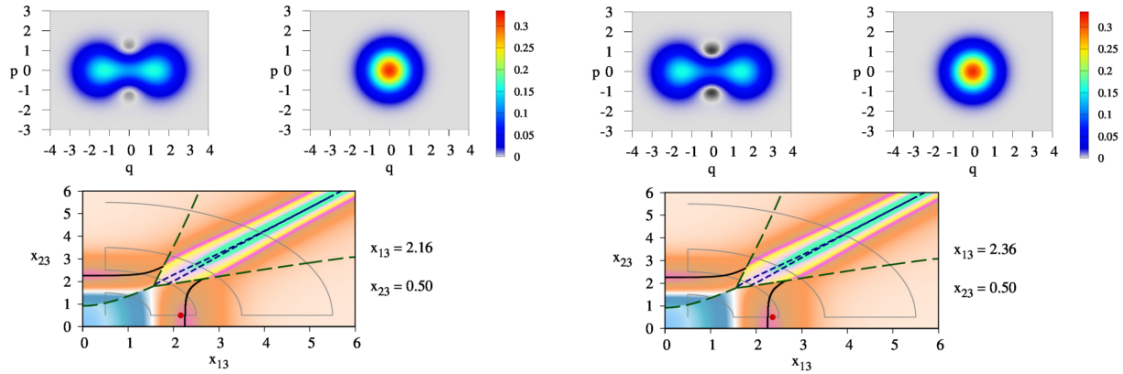


Figure 4: Behaviour of the Wigner function W_{13} and W_{23} , as the system goes through a stable-continuous transition. Regions where it becomes negative (black) reflect the existence of a superposition of states with different values of ν_{13} . (In each case, the continuous dim grey line is the evaluation trajectory, the red dot indicates the evaluation point in parameter space.) Note that, through this transition, W_{23} does not change.

128 We may plot these Wigner functions as functions of the field quadratures (q , p) at various
 129 points at either side of a separatrix, to see their behaviour as the system undergoes a phase
 130 transition [7].

131 Figure 4 shows the behaviour of W_{13} as the system goes through a stable-continuous tran-
 132 sition (red dot along a continuous grey evaluation trajectory). The elongation presenting a
 133 bimodal distribution is a consequence of photon contribution ν_{13} becoming significant. Re-
 134 gions where the Wigner function W_{13} is negative (black) appear as we move away from the
 135 normal region and cross the separatrix, because the number of photons in mode ν_{13} grows
 136 from zero: we now have a superposition of states with different values of ν_{13} .

137 Figure 5 shows the behaviour of both, W_{13} and W_{23} , as the system goes through an unstable-
 138 continuous transition (red dot along a continuous grey evaluation trajectory): close to the
 139 separatrix in dotted lines both photon contributions are significant. We note that both Wigner
 140 functions present elongated (bimodal) distributions. Above the separatrix the contribution of
 141 photons ν_{23} dominates and W_{23} has major regions with negative values; when the transition
 142 occurs, the field mode contributions to the ground state change their roles.

143 We see that the Wigner function characterises completely the phase diagram. In the nor-
 144 mal region the Wigner function describes a classical behaviour of the field (W takes positive
 145 values) and at least one photon mode remains in the vacuum, while the collective region is
 146 characterised by a Wigner function in which the quantumness of the photon modes is clearly
 147 shown; it divides itself into two regions, in each of which a single radiation mode dominates.

148 Videos showing the behaviour of the Wigner function for each mode, along the full trajec-
 149 tory shown in Figure 5, may be found for all the atomic configurations in the website of IOP
 150 *Physica Scripta*: [Ξ-configuration](#); [Λ-configuration](#); [V-configuration](#).

151 4.1 Correlation between Wigner Function and Entanglement

152 Bimodality and negativity of Wigner function reflect which field mode dominates in the super-
 153 radiant region, and not the parity of the state. This is evident when we compare it with an

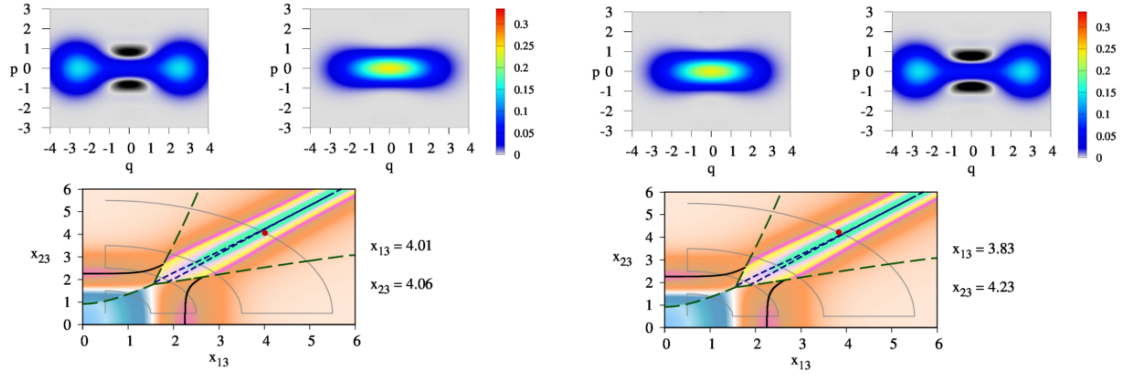


Figure 5: Behaviour of W_{13} and W_{23} as the system goes through an unstable-continuous transition. Across the transition the field mode contributions to the ground state change their roles $S_{13} \rightleftharpoons S_{23}$. (In each case, the continuous dim grey line is the evaluation trajectory, the red dot indicates the evaluation point in parameter space.)

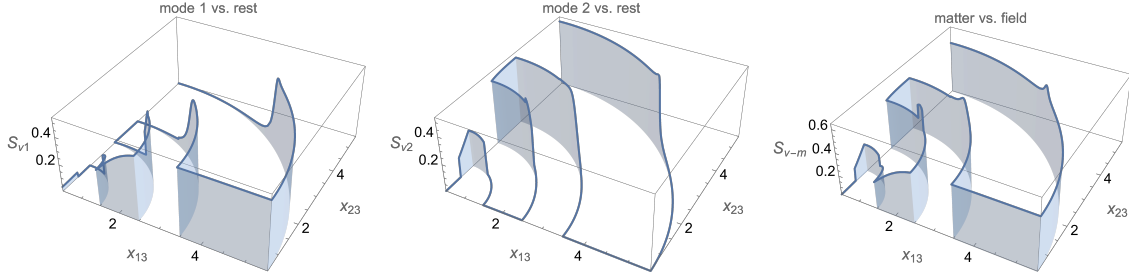


Figure 6: Plots of the different linear entropies S_{v1} , S_{v2} , and S_{v-m} , along a trajectory which crosses all detected transitions in parameter space.

154 entanglement measure (e.g., the linear entropy) [7]. We define

$$\begin{aligned} S_{v_1} &= 1 - \text{Tr}(\rho_{v_1}^2), \\ S_{v_2} &= 1 - \text{Tr}(\rho_{v_2}^2), \\ S_{v-m} &= 1 - \text{Tr}(\rho_{v_1 v_2}^2), \end{aligned}$$

155 to be, respectively, the linear entropy measuring correlation between field mode 1 and the rest
 156 of the system (matter + field mode 2), the linear entropy measuring correlation between field
 157 mode 2 and the rest of the system (matter + field mode 1), and the linear entropy measuring
 158 correlation between matter and field modes 1 and 2.

159 Figure 6 shows their plots along a trajectory which crosses all detected transitions in pa-
 160 rameter space. When the ground state is dominated by the vacuum state of the field (small
 161 values of the coupling parameters inside the Normal region), the correlation between one
 162 mode of the field, say i , and the rest of the system (matter + field mode j with $i \neq j$), is
 163 null $S_{L_i} = 0$ and the Wigner function is unimodal. This field-mode i vs. matter + field-mode
 164 j entanglement reaches its maximum as soon as we cross into the super-radiant region, the
 165 Wigner function showing negative values at a vicinity of the origin of quadrature q and small
 166 non-zero values of quadrature p . It then falls rapidly to zero as soon as we enter the region
 167 where field mode j dominates, even if a parity change is not had.

168 5 Conclusion

169 We have shown the results of the characteristics of the ground state for a single three-level
170 atom interacting dipolarly with a two-mode electromagnetic field. The symmetries of the
171 system allow for the division the quantum state space into subspaces which have a well-defined
172 parity. We have used a fidelity criterion to determine the quantum phase transitions for the
173 three three-level configurations.

174 We calculated the Wigner function for each of the electromagnetic modes Ω_{13} and Ω_{23} , and
175 showed the behaviour of these in various regions of the parameter space, which supplies fur-
176 ther evidence of the quantum phase transitions revealed by the fidelity criterion; the regions
177 where it takes negative values (the system exhibiting non-classical behaviour) were deter-
178 mined. Besides providing the phase transitions and a finer classification of them, it is interest-
179 ing to note that the Wigner function can be and has been measured experimentally [11, 12].

180 The linear entropy for all the subsystems was calculated and compared with the behaviour
181 of the Wigner function; we see that the entanglement between the substates responds to how
182 the bulk of the ground state changes from a subset of the basis with a major contribution from
183 one kind of photons, to a subset with a major contribution of the other one, and not to the
184 state parity even for large values of the coupling parameters.

185 Acknowledgements

186 **Funding information** This work was partially supported by DGAPA-UNAM (under projects
187 IN112520, and IN100120).

188 References

- 189 [1] S. Sachdev, *Quantum phase transitions*, Cambridge University Press (2011),
190 doi:[10.1017/CBO9780511973765](https://doi.org/10.1017/CBO9780511973765).
- 191 [2] S. Cordero, E. Nahmad-Achar, R. López-Peña and O. Castaños, *Polychromatic phase dia-*
192 *gram for n -level atoms interacting with ℓ modes of electromagnetic field*, Phys. Rev. A **92**
193 053843 (2015), doi:[10.1103/PhysRevA.92.053843](https://doi.org/10.1103/PhysRevA.92.053843).
- 194 [3] S. Cordero, E. Nahmad-Achar, O. Castaños and R. López-Peña, *A general system of*
195 *n levels interacting with ℓ electromagnetic modes*, Phys. Scr. **92** (4) 044004 (2017),
196 doi:[10.1088/1402-4896/aa6363](https://doi.org/10.1088/1402-4896/aa6363).
- 197 [4] R. Gilmore, *Catastrophe Theory for Scientists and Engineers*, Dover (New York, N.Y.)
198 (1993), ISBN 978-0471050643.
- 199 [5] P. Zanardi and N. Paunković, *Ground state overlap and quantum phase transitions*, Phys.
200 Rev. E **74**, 031123 (2006), doi:[10.1103/PhysRevE.74.031123](https://doi.org/10.1103/PhysRevE.74.031123).
- 201 [6] S.J. Gu, *Fidelity Approach to Quantum Phase Transitions*, Int. J. Mod. Phys. B **24** (23),
202 4371-4458 (2010), doi:[10.1142/S0217979210056335](https://doi.org/10.1142/S0217979210056335).
- 203 [7] R. López-Peña, S. Cordero, E. Nahmad-Achar, and O. Castaños, *Quantum phase diagrams*
204 *of matter-field Hamiltonians II: Wigner function analysis*, Phys. Scr. **96** 035103 (2021),
205 doi:[10.1088/1402-4896/abd654](https://doi.org/10.1088/1402-4896/abd654).

- 206 [8] S. Cordero, O. Castaños, R. López-Peña and E. Nahmad-Achar, *Reduced bases for a three-*
207 *level atom interacting with a two-mode radiation field*, Phys. Rev. A **99** 033811 (2019),
208 doi:[10.1103/PhysRevA.99.033811](https://doi.org/10.1103/PhysRevA.99.033811).
- 209 [9] V.V. Dodonov and V.I. Man'ko, *Evolution of Multidimensional Systems. Magnetic properties*
210 *of ideal gases of charged particles*, in *Invariants and the Evolution of Nonstationary Quantum*
211 *Systems*, (M.A. Markov, ed.), Nova Science Publishers (1989) ISBN: 0-941743-49-7.
- 212 [10] O. Castaños, S. Cordero, R. López-Peña and E. Nahmad-Achar, *Phase space proper-*
213 *ties of light within the generalised Dicke model*, Phys. Scr. **93** (8) 085102 (2018),
214 doi:[10.1088/1402-4896/aacd43](https://doi.org/10.1088/1402-4896/aacd43).
- 215 [11] G. Nogues, A. Rauschenbeutel, S. Osnaghi, P. Bertet, M. Brune, J. Raimond, S. Haroche,
216 L.G. Lutterbach, and L. Davidovich, *Measurement of a negative value for the Wigner func-*
217 *tion of radiation*, Phys. Rev. A **62** 054101 (2000), doi:[10.1103/PhysRevA.62.054101](https://doi.org/10.1103/PhysRevA.62.054101).
- 218 [12] K. Banaszek, C. Radzewicz, K. Wódkiewicz, K. and J.S. Kasiński, *Direct measure-*
219 *ment of the Wigner function by photon counting*, Phys. Rev. A **60** 674 (1999),
220 doi:[10.1103/PhysRevA.60.674](https://doi.org/10.1103/PhysRevA.60.674).